ELSEVIER

Journal of Alloys and Compounds 293–295 (1999) 93–100

Journal of ALLOYS AND COMPOUNDS

Hydrogenation behaviour, neutron diffraction studies and microstructural characterisation of boron oxide-doped Zr–V alloys

A.B. Riabov[a], V.A. Yartys[a,b], B.C. Hauback[b], P.W. Guegan[c], G. Wiesinger[d], I.R. Harris[c]

[a]*Metal Hydrides Department, Karpenko Physico-Mechanical Institute of the National Academy of Sciences of Ukraine, 5, Naukova Str., Lviv 290601, Ukraine*

[b]*Institute for Energy Technology, P.O. Box 40, Kjeller N-2027, Norway*

[c]*School of Metallurgy and Materials, The University of Birmingham, Edgbaston, Birmingham B15 2TT, UK*

[d]*Institute of Experimental Physics, TU Vienna, Wiedner Hauptstrasse 8/10, A-1040 Vienna, Austria*

Abstract

Compositions in the range $Zr_3V_3B_{0.12-0.40}O_{0.18-0.60}$ from the Zr–V–B_2O_3 system have been subjected to metallographic characterisation, microprobe analysis and powder neutron diffraction. On melting, boron was found to be reduced from its oxide and in the annealed condition, it was identified as a constituent of two phases, η-oxyboride Zr_3V_3(B,O) and vanadium boride V_3B_2. Hydrogen absorption–desorption properties were studied and related to the phase and structural composition of the alloys. A redistribution of the light atoms (oxygen, boron) within the η-oxyboride Zr_3V_3(B,O) matrix and, also, between the constituent phases of the alloys takes place during high temperature cycling in hydrogen which could indicate increased lattice mobility of these non-metallic elements in the hydride material.

Keywords: Zirconium; Vanadium; Boron oxide; Powder neutron diffraction

1. Introduction

Zr–V and Zr–V–Fe alloys belong to a group of efficient hydrogen absorbers [1,2]. The two-phase alloys formed when the Zr/V sequence is close to equiatomic, consist of α-Zr and a C15 Laves-phase compound ZrV_2 ($ZrV_{2-x}Fe_x$) [1]. Zr–V and Zr–V–Fe alloys doped with boron oxide modify the phase distribution, and an intermetallic compound with a cubic η-Fe_3W_3C structure type is formed [2]. The as-cast, B_2O_3 doped alloys have favourable hydrogenation properties. Hydrogen can easily be absorbed and the H-storage capacities are increased, exceeding 2.5 wt.% H [2]. The effect of the B_2O_3 addition on the hydrogenation behaviour in the Zr–V–B_2O_3 system is still not clear.

The present work focuses on studying the relationship between the structure and hydrogen absorption–desorption properties of the ZrV–B_2O_3 alloys.

2. Experimental details

The alloys were prepared from stoichiometric mixtures of high purity constituents, zirconium (99.97%), vanadium (99.5%) and boron oxide (99.9%), by arc melting in argon gas on a water cooled copper pad. The alloy specimens were remelted several times in order to improve sample homogeneity. Further annealing of the samples, placed inside evacuated, sealed quartz tubes, was performed at 1273 K for 14 days. The alloys were then quenched into iced water.

Sample characterisation was carried out by powder X-ray diffraction (XRD) [Philips PW1012 diffractometer, Cu Kα radiation].

B_2O_3 (99.98% ^{11}B-enriched) was used in order to avoid the high absorption of neutrons by natural boron. Powder neutron diffraction (PND) data were collected at $T=293$ K with the PUS instrument ($\lambda=1.5482$ Å; $2\Theta=10–130°$; $\Delta 2\Theta=0.05°$; 2400 data points) at the Institute for Energy Technology, Kjeller. The samples were contained in a sealed, cylindrical vanadium holder with a 5 mm inner

E-mail address: ALEXR@ah.ipm.lviv.ua (A.B. Riabov)

0925-8388/99/$ – see front matter
PII: S0925-8388(99)00306-0

diameter. The GSAS (General Structure Analysis System) software [3] was used in the Rietveld-type refinements. Nuclear scattering lengths were taken from the GSAS library (b_{Zr}=7.16, b_V=−0.38, b_O=5.80 fm) and from Ref. [4] (b_{11_B}=6.65 fm).

Scanning Electron Microscopy (SEM) [on JEOL 6300 and JEOL 840 instruments] was used for the characterisation of the microstructures and for microprobe element analysis.

Hydrogen absorption–desorption properties were studied using Temperature–Pressure Analysis (TPA) and Hydrogen Differential Thermal Analysis (HDTA) techniques at a heating rate of $5^\circ\,min^{-1}$. Purified hydrogen gas was supplied from a $LaNi_5$-based hydrogen storage unit. Powdered alloys for the neutron diffraction studies were obtained by a deuterium absorption–desorption cycle (initial gaseous pressure 1 bar; D_2 purity 99.8%). The synthesis of the deuterides was performed after a preliminarily vacuum activation of the alloys at 673 K.

3. Results and discussion

3.1. SEM and X-ray diffraction studies

A relatively small boron oxide doping [≤0.2 mol B_2O_3/(3Zr+3V)] increases the H-storage capacities compared to the mixed oxide Zr_3V_3O [1,5,6], see Fig. 1. The cell parameters are not changed significantly. However, increased B_2O_3 oxide contents [≥0.2 mol B_2O_3/(3Zr+3V)] gives a drastic reduction of both the H-contents and the cell parameters of this phase.

Detailed structural studies were carried out for two alloys with superior H-sorption characteristics, the stoichiometric compositions were $Zr_3V_3B_{0.24}O_{0.36}$ and $Zr_3V_3B_{0.40}O_{0.60}$. Boron oxide was not present in the as-cast alloys, indicating a complete redox type interaction with the ZrV melt. Several phase constituents were identified by microstructural studies and element analysis: solid solution of oxygen in zirconium α-ZrO_x, Laves type intermetallic λ$_2$-ZrV_2, η-oxyboride Zr_3V_3(B,O), $VO_{0.03}$ and its boride. Fig. 2 shows that annealing decreases the abundance of both α-ZrO_x and λ$_2$-ZrV_2, and, in parallel, increases the relative amount of η-Zr_3V_3(B,O). The oxyboride becomes the matrix phase (see Fig. 2b and c), growing from initial thin intergranular layers (see Fig. 2a). This indicates that both α- and λ$_2$-phases are involved in the peritectoid interaction resulting in the formation of the η-phase.

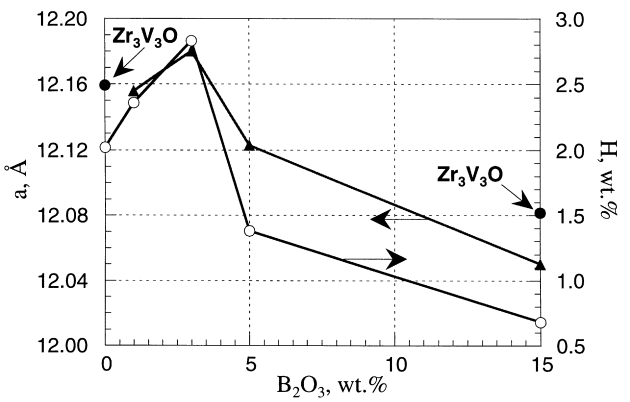

Fig. 1. Cell parameters and H-storage capacities for the $Zr_{55}V_{40}Fe_5$–B_2O_3 alloys versus boron oxide content [1]. Reference data for Zr_3V_3O [5,6] are shown for comparison.

From elemental analysis (Zr: O~3.3: 1) and XRD data, the oxygen content in α-ZrO_x was estimated to be Zr_3O, which is the limiting value for the continuous solid solution of O in α-Zr [7]. The upper limits of the cell parameters of the hexagonal unit cell of α-ZrO_x (a= 3.243(4)–3.257(1) Å; c=5.185(3)–5.209(4) Å) from the XRD data are larger than the corresponding reference values for Zr_3O ($a_{subcell}=a/\sqrt{3}$=3.2502; c=5.1975 Å [7]). It is believed, due to the relationship between the O-contents and the unit cell parameters in α-ZrO_x, that the oxygen concentration probably exceeds 25 at.%. Further investigations of the binary Zr–O system are necessary to clarify this suggestion. The present Rietveld refinements were based on the literature crystal structure data for Zr_3O [8].

The elemental analysis of the annealed $Zr_3V_3B_{0.40}O_{0.60}$ alloy showed that both boron and oxygen participate in the formation of η-Zr_3V_3(B,O) oxyboride. A complex nitride $Zr_7V_5N_2$ with the Fe_3W_3C type structure was found previously in the Zr–V–N system [9], and a formation of a mixed η-type oxynitride Zr_3V_3(N,O) with two non-metallic elements present, was reported earlier [1,10]. We have not found any published data on the formation of B-containing η-phases in the Zr–V system.

Vanadium boride is the second boron-containing compound in the $Zr_3V_3B_{0.24-0.40}O_{0.36-0.60}$ system. It has a smaller grain size than the other constituent phases (see Fig. 2). By XRD it was determined as V_3B_2. Quantitative phase analysis of the PND pattern showed the fraction of this phase in the multiphase samples (the data are presented below).

From the SEM and XRD data, the following reactions in the Zr–V–B_2O_3 system can be proposed:

(a) Reduction of the boron oxide on melting the alloy:

$$Zr + V + B_2O_3 \Rightarrow Zr_3O + Zr_3V_3(B, O) + V_3B_2$$

(b) Peritectic formation of the Laves λ$_2$-ZrV_2 phase during solidification of the as-cast alloy and during annealing:

$$Zr + 2\,V \Rightarrow ZrV_2$$

(c) High-temperature (peritectoid) synthesis of the η-phase during annealing:

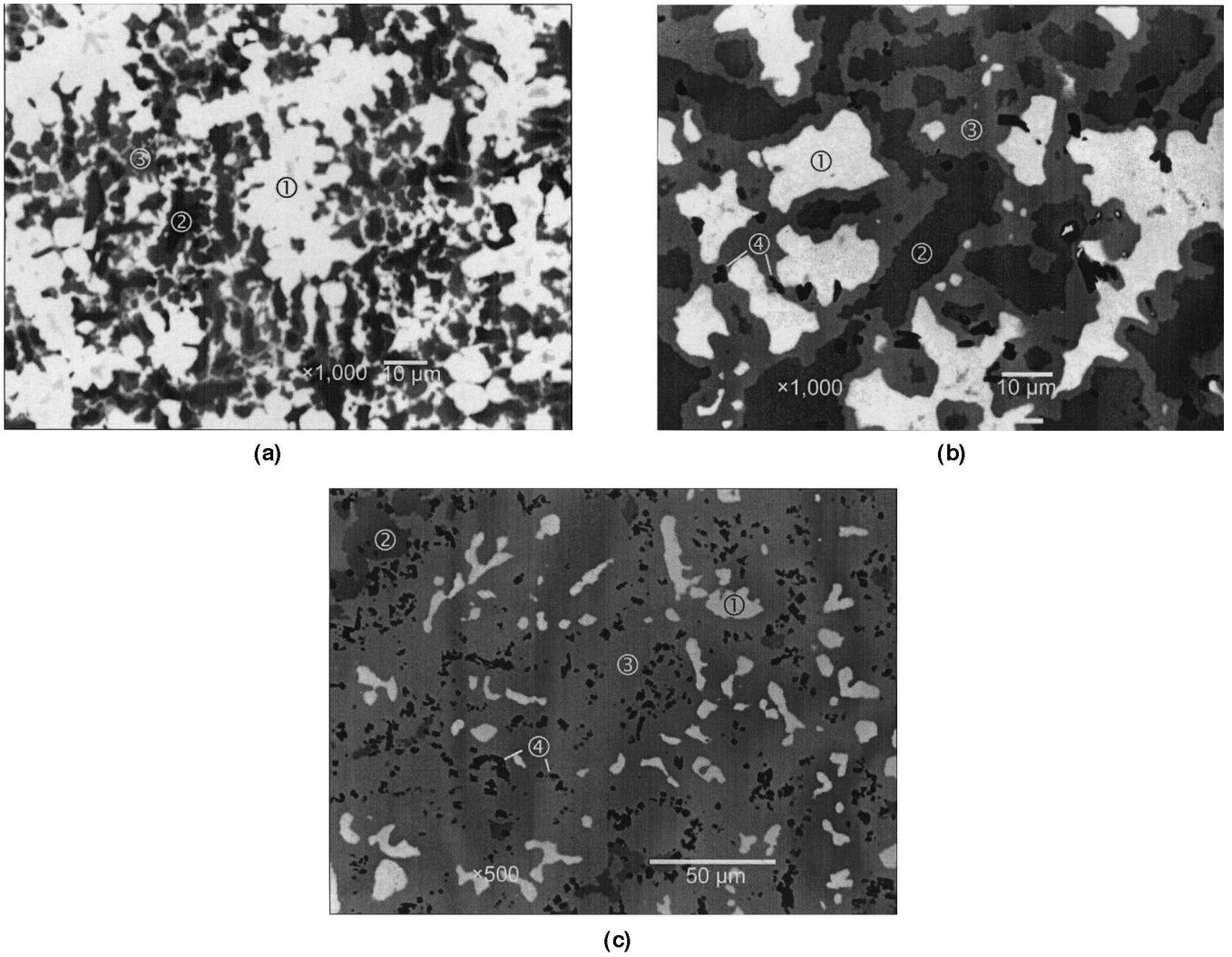

Fig. 2. SEM images of the $Zr_3V_3B_{0.12}O_{0.18}$ (a, as-cast; b, annealed) and $Zr_3V_3B_{0.40}O_{0.60}$ (c, annealed) alloys. Phase constituents: 1 – Zr_3O; 2 – λ_2-ZrV_2; 3 – η-$Zr_3V_3(B,O)$; 4 – $VO_{0.03}/V_3B_2$.

$$ZrV_2 + Zr_3O + V_3B_2 \Rightarrow Zr_3V_3(B, O)$$

3.2. Powder neutron diffraction studies

Observed, calculated and difference PND profiles for the $Zr_3V_3B_{0.24}O_{0.36}$ and $Zr_3V_3B_{0.40}O_{0.60}$ alloys are shown in Fig. 3a and b. Table 1 presents coordinates, temperature factors and *R*-factors from the Rietveld-type analysis for two η-oxyborides. Zr and V atoms are completely ordered with Zr occupying the 48*f* sites and V in both the 32*e* and 16*c* sites. In $Zr_3V_3B_{0.24}O_{0.36}$, the non-metallic atoms, O and B, completely occupy only one site, namely the distorted octahedra Zr_6. These data are in good agreement with previously published results for the η-Zr_3V_3O oxide [6].

In $Zr_3V_3B_{0.40}O_{0.60}$, the 8*b* sites start to fill by O/B atoms (population of 4%), in addition to the ~94% occupation of the 16*d* positions (see Table 1).

Since the neutron scattering lengths are not significantly different for O and ^{11}B (5.80 and 6.65 fm, respectively), it was not possible to determine the relative abundance of these elements in the η-oxyborides. Further studies are necessary to clarify this point; a mixture of $^{10}B_2O_3$ and $^{11}B_2O_3$ can be used to distinguish the contribution from O and B in the overall scattering.

In contrast to the nearly 100% occupancy of the distorted Zr_6 16*d* sites in the alloy, these octahedra are only partially filled in saturated deuteride (~30% in the $Zr_3V_3B_{0.40}O_{0.60}$-based η-deuteride). The regular 8*b* Zr_6 octahedra are completely occupied by inserted atoms in the deuteride. These results can be interpreted presumably in terms of the redistribution of the inserted atoms during the absorption–desorption cycling. Complete PND data for the $Zr_3V_3B_{0.24}O_{0.36}$- and $Zr_3V_3B_{0.40}O_{0.60}$-based deuterides will be published separately [11].

Relative phase fractions of the existing phase constituents, η-$Zr_3V_3(B,O)$, Zr_3O, V_3B_2, $VO_{0.03}$ and ZrV_2 ($ZrV_{2-x}B_x$) determined from the quantitative phase analy-

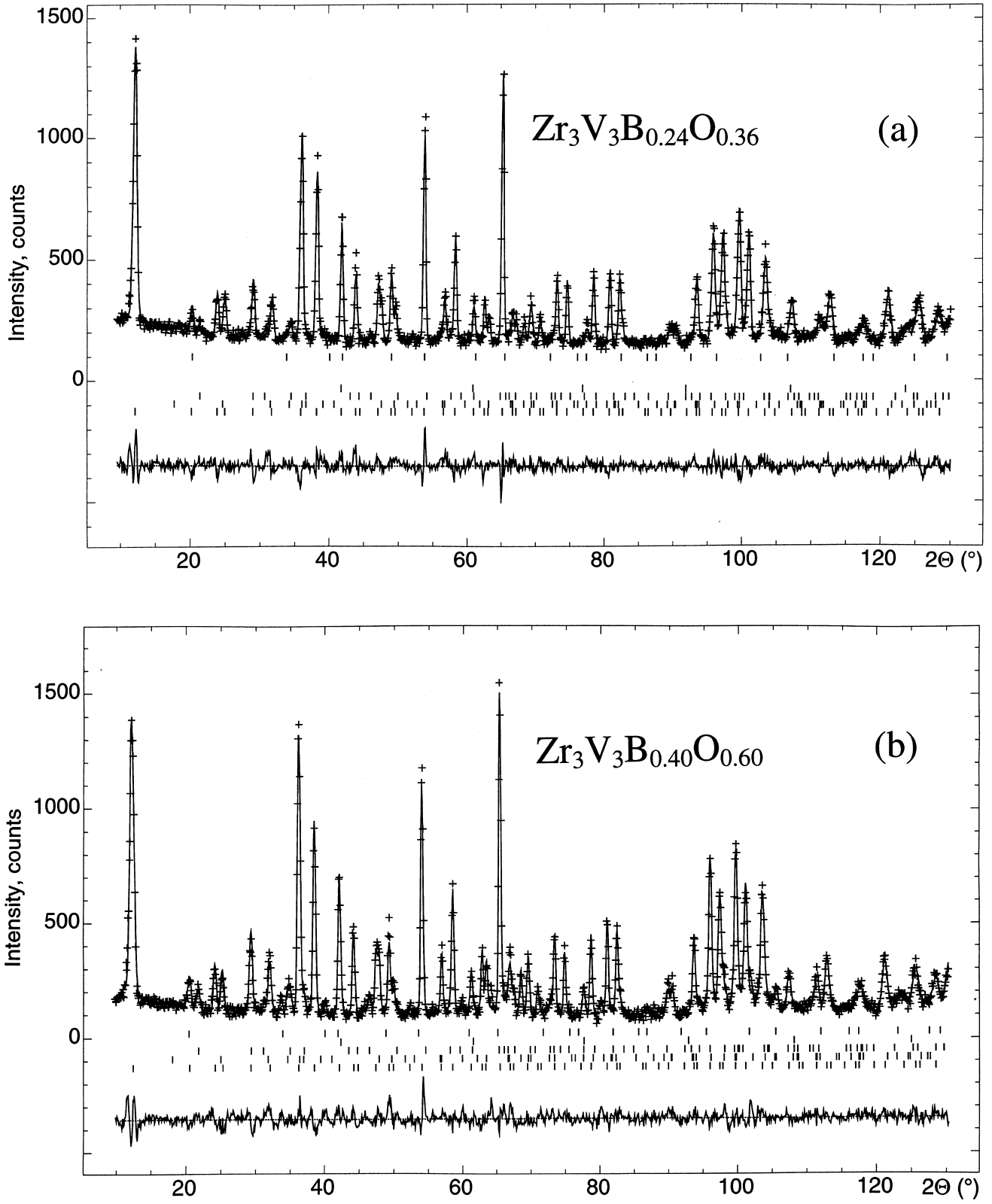

Fig. 3. Observed (+), calculated (upper line) and difference (lower line) powder neutron diffraction profile for $Zr_3V_3B_{0.24}O_{0.36}$ (a) and $Zr_3V_3B_{0.40}O_{0.60}$ (b) alloys after one deuterium absorption–desorption cycle. The positions of the peaks of the constituent phases are marked (from bottom to top): $Zr_3V_3(B,O)$, Zr_3O, V_3B_2, $VO_{0.03}$, λ_2-ZrV_2 (λ_2-$ZrV_{2-x}B_x$).

Table 1
Atomic coordinates and temperature factors (in 10^{-2}Å^2) for the $Zr_3V_3(B,O)$ η-oxyboride from the Rietveld refinements of the PND data for the $Zr_3V_3B_{0.24-0.40}O_{0.36-0.60}$ alloys after proceeding through one deuterium absorption–desorption cycle

Alloy	Atom	Site	x	y	z	U_{iso}	Occupancy
$Zr_3V_3B_{0.24}O_{0.36}$ [a]	Zr	48*f*	0.5636(2)	3/8	3/8	0.59(5)	1.00(–)
	V1	16*c*	0	0	0	0.5(–)	1.00(–)
	V2	32*e*	0.204(2)	0.204(2)	0.204(2)	0.5(–)	1.00(–)
	(O+B) [b]	16*d*	1/2	1/2	1/2	0.9(1)	1.08(2) [c]
$Zr_3V_3B_{0.40}O_{0.60}$ [d]	Zr	48*f*	0.5648(2)	3/8	3/8	0.99(4)	1.00(–)
	V1	16*c*	0	0	0	2.2(16)	1.00(–)
	V2	32*e*	0.203(2)	0.203(2)	0.203(2)	1.0(–)	1.00(–)
	(O+B) [b]	16*d*	1/2	1/2	1/2	1.14(9)	0.94(1)
	(O+B) [b]	8*b*	7/8	3/8	7/8	2.0(–)	0.04(1)

[a] $Zr_3V_3B_{0.24}O_{0.36}$: Space group $Fd\bar{3}m$; $a=12.1607(2)$ Å; $R_p=0.063$; $R_{wp}=0.080$; $\chi^2=1.55$.
[b] In the refinements $^{11}B/O$ sequence was kept equal to 2:3, as in the doping boron oxide.
[c] More than 100% occupancy indicates increased population of the 16*d* sites by ^{11}B.
[d] $Zr_3V_3B_{0.40}O_{0.60}$: Space group $Fd\bar{3}m$; $a=12.1705(4)$ Å; $R_p=0.061$; $R_{wp}=0.078$; $\chi^2=1.88$.

sis of the PND data (Table 2), are consistent with the alloy microstructures. The weight fractions of Zr_3O and V_3B_2 in the alloys were found to rise with increased doping (see Table 2).

Good agreement between the derived crystallographic characteristics of the present phases and the reference data should be noted from Table 3. In the refinements, the Zr_3O suboxide was described as having a hexagonal superstructure with $a \sim a_{\alpha\text{-}Zr} \times \sqrt{3}$; $c \sim c_{\alpha\text{-}Zr}$ [8] and oxygen atoms filling every third Zr_6 octahedron regularly. No variations of oxygen contents were allowed. Similarly, oxygen content was also fixed in VO_x to $x=0.03$, which is equal to the value reported in the literature [12]. In the case of V_3B_2, the refined atomic coordinates for the vanadium and boron atoms have been found to be close to those for the uranium and silicon atoms in the U_3Si_2 compound [13]. Finally, in the case of the $Zr_3V_3B_{0.24}O_{0.36}$ alloy, a measured cell parameter for the λ_2-phase is lower with respect to ZrV_2, which agrees with a suggestion of possible substitution of ~ 5% of vanadium by smaller boron atoms (see Table 3 for the details).

Table 2
Relative abundance of the phase constituents in the $Zr_3V_3B_{0.24-0.40}O_{0.36-0.60}$ alloys after proceeding through one deuterium absorption–desorption cycle determined by quantitative analysis of the PND data

Phase	Relative abundance, wt.%	
	$Zr_3V_3B_{0.24}O_{0.36}$	$Zr_3V_3B_{0.40}O_{0.60}$
η-$Zr_3V_3(B,O)$	84.9(–)	79.5(–)
Zr_3O	8.5(4)	11.7(2)
V_3B_2	3.7(4)	6.4(3)
$VO_{0.03}$	0.6(1) [a]	1.1(1) [a]
ZrV_2		1.3(3)
$ZrV_{2-x}B_x$	2.3(3)	

[a] The relative amount of $VO_{0.03}$ was limited to be equal to the content of VD_2 in the deuterated alloy (the latter was derived from Rietveld refinements of the PND data for the corresponding deuterides). Without constraints, the phase fraction of $VO_{0.03}$ in the deuterium-free samples appeared to be inconsistent with the microstructural characterisation and XRD studies of the alloys, observed here to be increased significantly due to a small value of the neutron scattering length of vanadium.

3.3. Hydrogen absorption–desorption properties

Hydrogen absorption properties of annealed $Zr_3V_3B_{0.12-0.40}O_{0.18-0.60}$ differ significantly from the as-cast alloys. After annealing, hydrogen absorption starts at 605–630 K, as shown by the TPA and HDTA measurements (see Fig. 4). This unexpected low hydrogenation activity contrasts with the behaviour of these alloys in the as-cast condition [1,2]. Oxygen atoms are probably redistributed in the alloys during annealing, with an increased concentration in the intergranular areas, thus blocking the low-temperature hydrogenation.

In the TPA study, the $Zr_3V_3B_{0.40}O_{0.60}$ sample was heated above 630 K to ~ 1010 K, and no further absorption was observed, see Fig. 4. This suggests that no disproportionation of the η-oxyboride metal matrix takes place during the experiment. This was confirmed by the XRD data, and is in contrast to the slight disproportionation observed under similar P–T conditions for the isostructural mixed oxide $Zr_4Fe_2O_{0.6}$ [16,17].

Hydride decomposition proceeds continuously under vacuum over a wide temperature range from room temperature to approximately 960 K, with peaks at 500 K and at 810 K, see Fig. 5. Hydrogen desorption from the η-oxyboride and the other phases was completed in the course of these experiments, as after desorption, the unit cell parameters agree well with the initial, non-hydrogenated alloys. Similar behaviour was reported earlier for the hydrogenated η-oxide Zr_3V_3O [18].

A small amount of a new phase constituent, the face centred cubic zirconium (boro)oxide is formed during the high temperature deuterium desorption (see Fig. 6), possibly indicating an increased mobility of the non-metallic atoms when hydrogen (deuterium) is present.

Increased oxide doping decreases the thermal stability of the hydrides formed. Fig. 7 shows that the second H-

Table 3
Crystallographic data for the minor phase constituents in the $Zr_3V_3B_{0.24-0.40}O_{0.36-0.60}$ alloys after proceeding through one deuterium absorption–desorption cycle (from Rietveld refinements of the PND data)

	Reference data	$Zr_3V_3B_{0.24}O_{0.36}$	$Zr_3V_3B_{0.40}O_{0.60}$
Zr_3O	Space group $P6_322$; $a=5.6295$; $c=5.1975$ Å; 6 Zr in 6*g*: 0.333, 0, 0; 2 O in 2*c*: 1/3, 2/3, 1/4 [8]	Space group $P6_322$; $a=5.6172(7)$; $c=5.185(1)$ Å; 6 Zr in 6*g*: 0.3333(–), 0, 0; $U_{iso}=0.1(2)$ Å^2; 2 O in 2*c*: 1/3, 2/3, 1/4; $U_{iso}=0.2(4)$ Å^2	Space group $P6_322$; $a=5.6308(5)$; $c=5.1898(7)$ Å; 6 Zr in 6*g*: 0.3333(–), 0, 0; $U_{iso}=1.0(1)$ Å^2; 2 O in 2*c*: 1/3, 2/3, 1/4; $U_{iso}=4.6(6)$ Å^2
V_3B_2	Space group $P4/mbm$; Structure type: U_3Si_2; $a=5.728$–5.739; $c=3.028$–3.030 Å; atomic coordinates are not given [12,13]. U_3Si_2 structure type [14]: Space group $P4/mbm$; $a=7.3299(4)$; $c=3.9004(5)$ Å 2 U1 in 2*a*: 0, 0, 0; 4 U2 in 4*h*: *x*, 1/2+*x*, 1/2; $x=0.181$. 4 Si in 4*g*: *x*, 1/2+*x*, 0; $x=0.389$	Space group $P4/mbm$; $a=5.755(2)$; $c=3.038(2)$ Å; 2 V1 in 2*a*: 0, 0, 0; $U_{iso}=1.0(–)$ Å^2; 4 V2 in 4*h*: *x*, 1/2+*x*, 1/2; $x=0.17(3)$; $U_{iso}=1.0(–)$ Å^2; 4 B in 4*g*: *x*, 1/2+*x*, 0; $x=0.388(3)$; $U_{iso}=1.9(6)$ Å^2	Space group $P4/mbm$; $a=5.746(2)$; $c=3.036(1)$ Å; 2 V1 in 2*a*: 0, 0, 0; $U_{iso}=1.0(–)$ Å^2; 4 V2 in 4*h*: *x*, 1/2+*x*, 1/2; $x=0.17(2)$; $U_{iso}=1.0(–)$ Å^2; 4 B in 4*g*: *x*, 1/2+*x*, 0; $x=0.390(2)$; $U_{iso}=2.0(–)$ Å^2
$VO_{0.03}$	Space group $Im\bar{3}m$; $a=3.048$ Å [15]; 2 V in 2a: 0, 0, 0; 0.06 O in 6*b*: 1/2, 1/2, 0	Space group $Im\bar{3}m$; $a=3.043(1)$ Å; 2 V in 2*a*: 0, 0, 0; $U_{iso}=1.0(–)$ Å^2; 0.06(–) O in 6*b*: 1/2, 1/2, 0; $U_{iso}=2.0(–)$ Å^2	Space group $Im\bar{3}m$; $a=3.028(2)$ Å; 2 V in 2*a*: 0, 0, 0; $U_{iso}=1.0(–)$ Å^2; 0.06(–) O in 6*b*: 1/2, 1/2, 0; $U_{iso}=2.0(–)$ Å^2
ZrV_2	Space group $Fd\bar{3}m$; $a=7.448(3)$ Å; 8 Zr in 8*a*: 1/8, 1/8, 1/8; 16 V in 16*d*: 1/2, 1/2, 1/2 [15]		Space group $Fd\bar{3}m$; $a=7.482(6)$ Å; 8 Zr in 8*a*: 1/8, 1/8, 1/8; $U_{iso}=1.0(–)$ Å^2; 16 V in 16*d*: 1/2, 1/2, 1/2; $U_{iso}=1.0(–)$ Å^2
$ZrV_{2-x}B_x$		Space group $Fd\bar{3}m$; $a=7.412(3)$ Å; 8 Zr in 8*a*: 1/8, 1/8, 1/8; $U_{iso}=1.0(–)$ Å^2; 15.2 (–) V in 16*d*: 1/2, 1/2, 1/2; $U_{iso}=1.0(–)$ Å^2; 0.8(16) B in 16*d*: 1/2, 1/2, 1/2; $U_{iso}=1.0(–)$ Å^2	

desorption peak shifts gradually from 893 to 723 K when the amount of oxide increases. It is reasonable to assume that the (O+B) contents increases in the metal matrix in parallel with the amount of B_2O_3 involved in the interaction. From this it can be concluded that the dissolution of the non-metallic elements decreased the hydride's stability.

Finally, the onset of hydrogen desorption was found to depend significantly on the history of the hydride. Hydrides, decomposed in situ after synthesis, start to desorb hydrogen already at room temperature (Fig. 5), whereas even short exposure to air poisons their surface and suppresses the near-room temperature desorption. For these poisoned hydrides, the hydrogen desorption starts at noticeably higher temperatures, 373–423 K (desorption traces not shown).

In conclusion, boron and oxygen were found to be involved in the formation of the η-type compound $Zr_3V_3(B,O)$, which is the matrix phase of the boron oxide

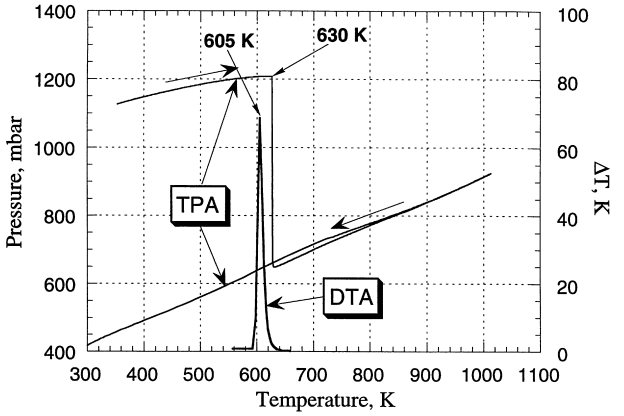

Fig. 4. TPA and HDTA traces of the hydrogen absorption for the $Zr_3V_3B_{0.40}O_{0.60}$ alloy.

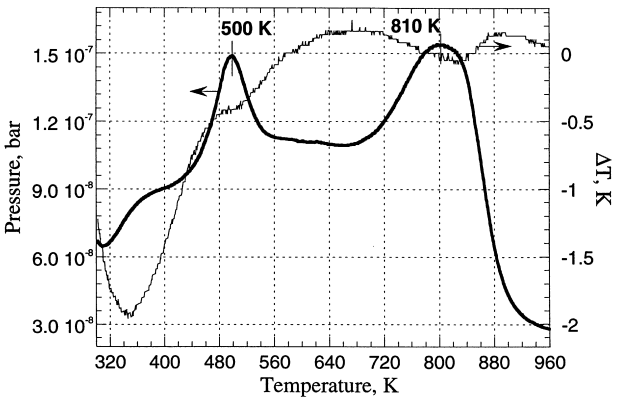

Fig. 5. HDTA traces of the hydrogen desorption from the $Zr_3V_3B_{0.40}O_{0.60}$-based saturated (1 bar H_2) hydride.

doped and annealed ZrV alloys. H-storage capacity and thermal stability of their hydrides are strongly influenced by the B_2O_3 contents. No disproportionation of the η-oxyboride $Zr_3V_3(B,O)$ occurs in hydrogen gas (1 bar H_2) at temperatures up to 1010 K, indicating a high thermo-

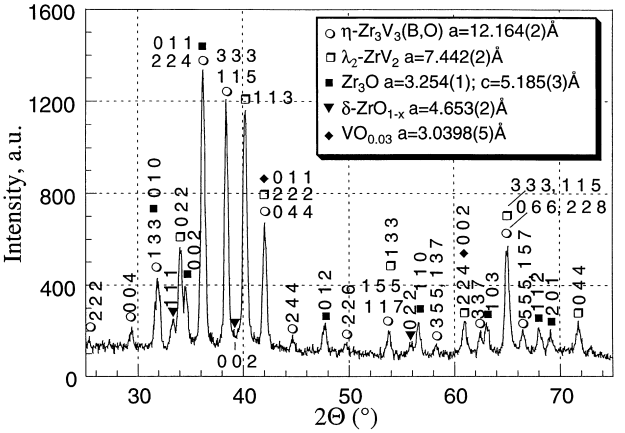

Fig. 6. XRD pattern of the $Zr_3V_3B_{0.12}O_{0.18}$ alloy after one hydrogen absorption–desorption cycle.

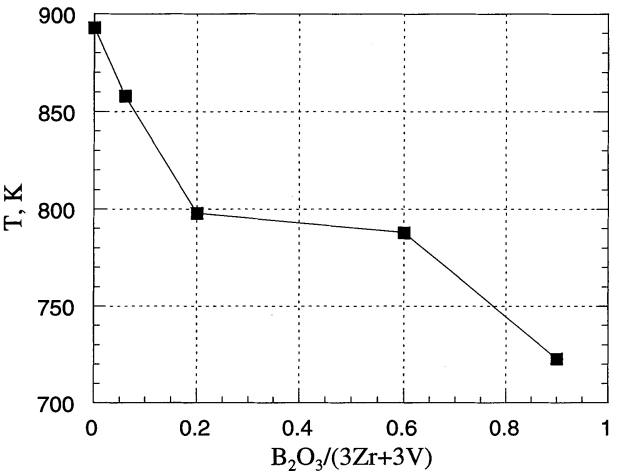

Fig. 7. The dependence of the high temperature peak of hydrogen desorption on the amount of B_2O_3 doping in the ZrV alloys.

dynamic stability of the metal matrix. Instead, a redistribution of the light non-metallic atoms (O,B) in the lattice of the η-oxyboride proceeds in the high temperature region, showing that their mobility could be increased in the hydride.

Acknowledgements

The authors (ABR, VAY, PWG and IRH) would like to thank the Royal Society for the provision of a research grant supporting a collaborative research program between the PhMI NAS of Ukraine and the School of Metallurgy and Materials, The University of Birmingham. G.W. acknowledges the support of the Austrian Science Foundation (grant #5566). This work was supported in part by the Norwegian Research Council and Hydro Megon.

References

[1] V.A. Yartys, I.Yu. Zavaliy, M.V. Lototsky, Koordinatsionnaya Kimiya (Soviet Journal of Coordination Chemistry) 18 (4) (1992) 409.
[2] V.A. Yartys, I.Yu. Zavaliy, M.V. Lototsky, A.B. Riabov, Yu.F. Shmalko, Z. Phys. Chem. 183 (1994) 465.
[3] A.C. Larson, R.B. von Dreele, General Structure Analysis System, LANL, 1994.
[4] V.F. Sears, Neutron News 3 (1992) 26.
[5] I.Yu. Zavaliy, A.B. Riabov, V.A. Yartys, J. Alloys Comp. 219 (1995) 34.
[6] F.J. Rotella, H.E. Flotow, D.M. Gruen, J.D. Jorgensen, J. Chem. Phys. 79 (1983) 4522.
[7] L.E. Fykin, R.P. Ozerov, V.P. Smirnov, S.P. Solovyov, V.V. Sumin, Metallidy. Stroyeniye, svoystva, primeneniya (Metallides. Structure, properties, applications), Nauka, Moscow, 1971.
[8] B. Holmberg, T. Dagerhamn, Acta Chem. Scand. 15 (1961) 919.

[9] H. Holleck, F. Trümmler, Monatsh. Chem. 98 (1967) 133.
[10] M.V. Lototsky, PhD Thesis, Lviv, 1992.
[11] V.A. Yartys, A.B. Riabov, B.C. Hauback, to be submitted to J. Alloys Comp.
[12] E. Rudy, F. Benessovsky, L. Toth, Z. Metallkunde 54 (1963) 345.
[13] R.E. Spear, P.W. Gilles, High Temp. Sci. 1 (1969) 86.
[14] W.H. Zahariasen, Acta Crystallogr. 1 (1948) 265.
[15] P. Villars, L.D. Calvert (Eds.), Pearson's Handbook of Crystallographic Data for Intermetallic Phases, Vols. 1–3, American Society for Metals, Ohio, 1985, 5087 p.
[16] V.A. Yartys, H. Fjellvåg, I.R. Harris, B.C. Haubck, A.B. Riabov, M. Sørby, I.Yu. Zavaliy, J. Alloys Comp., this issue.
[17] V.A. Yartys, I.Yu. Zavaliy, A.B. Riabov, P.W. Guegan, J.C. Clarke, I.R. Harris, B.C. Hauback, H. Fjellvag, in: T.O. Saetre (Ed.), Hydrogen Power: Theoretical and Engineering Solutions, Proceedings of the International Symposium HYPOTHESIS II, Grimstad, Norway, 18–22 August 1997, Kluwer Academic Publishers, The Netherlands, 1998, p. 303.
[18] A.B. Riabov, PhD Thesis, Lviv, 1997.